Statistical Prediction and Measurement of Induced Voltages on Components Within Complicated Enclosures: A Wave-Chaotic Approach

Sameer Hemmady, *Member, IEEE*, Thomas M. Antonsen, Jr., *Fellow, IEEE*, Edward Ott, *Life Fellow, IEEE*, and Steven M. Anlage, *Member, IEEE*

***Abstract*—We consider induced voltages on electronic components housed inside complicated enclosures and subjected to high-frequency radiation. The enclosure is assumed to be large compared to the wavelength in which case there is strong dependence of wave properties (eigenvalues, eigenfunctions, scattering, and impedance matrices, etc.) on small perturbations. The source(s) and sink(s) of radiation are treated as generalized ports and their coupling to the enclosure is quantified by an appropriate nonstatistical radiation impedance matrix. The field fluctuations within the enclosure are described in a statistical sense using random matrix theory. The random matrix theory approach implies that the wave fluctuations have "universal" properties in the sense that the statistical description of these properties depends only upon the value of a single, experimentally accessible, dimensionless loss parameter. We formulate a statistical prediction algorithm for the induced voltages at specific points within complicated enclosures when subjected to short-wavelength electromagnetic (EM) energy from either external or internal sources. The algorithm is tested and verified by measurements on a computer box. The insights gained from this model suggest design guidelines for enclosures to make them more resistant to disruptive effects produced by a short-wavelength EM radiation.**

***Index Terms*—Electromagnetic (EM) compatibility, high-power microwave effects, overmoded cavities, radiation impedance, ray chaos, statistical electromagnetism, wave scattering.**

I. Introduction

CHARACTERIZING the nature of short-wavelength electromagnetic (EM) field quantities within large complicated enclosures connected to multiple ports (avenues of ingress or egress of EM energy) poses a unique challenge in the field of EM compatibility and microwave engineering. This problem manifests itself in many situations such as wireless-signal penetration into rooms or buildings [1], specious EM emissions from personal electronic devices inside aircraft fuselages [2]–[4], or the upset of sensitive electronic systems due to intentional EM interference threats [5], [6]. The abundance of such situations has motivated a significant research effort to identify, quantify, and eventually predict the nature of short-wavelength EM field quantities within large complicated enclosures. Currently, this effort can be broadly classified into two approaches, one that may be described as deterministic and another that may be described as statistical.

The deterministic approach makes use of sophisticated numerical analysis techniques to estimate the value of the EM field quantities at specific locations within the enclosure of interest, such as a room, aircraft fuselage, or computer box. In this approach, the exact geometry of the ports, which "drive" the enclosure as well as the geometry and location of objects or components within the enclosure are typically modeled using a CAD software tool. The numerical analysis software then solves the relevant wave equations subject to appropriate boundary conditions for the desired EM field quantities within the enclosure. This deterministic approach has been facilitated by significant advances in the areas of computer hardware, computational EMs, numerical analysis techniques, and data processing capabilities. In certain laboratory-type scenarios, it is now possible to make deterministic predictions of short-wavelength EM field quantities inside electrically large enclosures, and these predictions agree reasonably well with experimental measurements [7].

In a specific application, it is not always possible to identify or accurately model the geometry of all the driving ports and the location of all the objects within the enclosure. Moreover, when the wavelength of the EM radiation becomes much smaller than the size of the enclosure and/or the EM environment becomes very dense, such as within the avionics bay of an aircraft where several electrical cables lie in close proximity to one another, the computational time and resources required for a deterministic solution to the EM field quantities of interest can be quite prohibitive. In such large complicated enclosures, the nature of the bounded short-wavelength EM field quantities show strong fluctuations that are extremely sensitive to the detailed shape of the enclosure (which behaves as a cavity resonator), the

Manuscript received March 17, 2011; revised August 29, 2011; accepted November 1, 2011. Date of publication January 4, 2012; date of current version August 17, 2012. This work was supported by the Department of Defense Multidisciplinary University Research Initiative (MURI) for the study of microwave effects under the Air Force Office of Scientific Research (AFOSR) Grant F496200110374, AFOSR DURIP Grants FA95500410295 and FA95500510240, AFOSR Grants FA95500710049, FA95501010106, ONR/UMD AppEl Center, task A2 Grant N000140911190, and by the Israel/USA Binational Science Foundation.

S. Hemmady is with the TechFlow Scientific, A Division of TechFlow Inc., Albuquerque, NM 87111 USA and also with the Department of Electrical and Computer Engineering, University of New Mexico, Albuquerque, NM 87131 USA (e-mail: shemmady@techflow.com).

T. M. Antonsen, Jr. and E. Ott are with the Department of Physics, Department of Electrical and Computer Engineering, and the Institute for Research in Electronics and Applied Physics, University of Maryland, College Park, MD 20742 USA (e-mail: antonsen@umd.edu; edott@umd.edu).

S. M. Anlage is with the Department of Physics, Department of Electrical and Computer Engineering, and the Center for Nanophysics and Advanced Materials, University of Maryland, College Park, MD 20742 USA (e-mail: anlage@umd.edu).

Digital Object Identifier 10.1109/TEMC.2011.2177270

orientation of internal objects (which act as scattering features), the frequency of the radiation, and the exact geometry of the ports. Minute changes in the shape of the enclosure, such as contractions or expansions due to ambient thermal fluctuations, mechanical vibrations, or the reorientation of an internal component or cable, can result in significantly different EM environments within the enclosure. Thus, even a deterministic solution to the EM response of the enclosure for one configuration may not provide useful information for predicting that of another nearly identical configuration. Hence, a probabilistic approach is called for which treats the bounded EM field quantities as random variables and the nature of their fluctuations characterized by suitable probability density functions (PDFs). This approach has spawned the field of statistical electromagnetism [8].

Researchers in the field of statistical electromagnetism create probabilistic models for the PDFs of EM field fluctuations within large complicated enclosures making certain assumptions about the nature of the EM wave scattering within the enclosure. For instance, it is assumed that these EM field fluctuations arise purely because of the nature of the short-wavelength plane waves randomly bouncing within the complicated large enclosure (a statistical condition called the "random plane wave hypothesis" [9]). The inclusion of these assumptions into the statistical models has led to several "universal" predictions for the PDF of EM fields at a point, the correlation function of fields at two points near each other, the Q of the enclosure, and the statistics for the scattering properties within the enclosure [8], [10]–[16]. By "universal" we mean that the shapes and scales of the PDFs are not dependent on the exact shape of the enclosure or the location of the scatters within the enclosure, but rather are parameterized by a single global quantity that characterizes loss within the enclosure.

Researchers have also been successful in experimentally validating the existence of these universal fluctuations using mode-stirred chambers [17], [18] that inherently possess the necessary wave-scattering properties to produce such universal fluctuations [19], once it is experimentally ensured that the driving ports are perfectly coupled to the enclosure. By "perfect coupling" we mean that a wave incident on the port from outside the enclosure is entirely transmitted into the enclosure experiencing no prompt reflection. Here, we envision such an incident wave to arrive at the port through a connecting external transmission line, where the external transmission line may be an actual physical transmission line or a mathematical construct in which several incident modal waves are represented as arriving at the port via equivalent transmission lines. Thus, in the perfect coupling case, any reflected waves in these transmission lines originate from waves that have entered the enclosure, bounced within it, and returned to the port. Though the condition of "perfect coupling" may be achieved under special circumstances, this is generally not the case. Typically, the presence of mismatched driving ports leads to system-specific artifacts in the measured EM field fluctuations at the ports, thereby leading to deviations from the predicted "universal" fluctuations. Thus, when it comes to the problem of predicting short-wavelength EM field quantities at ports in large complicated enclosures, one should consider a statistical model that utilizes the universal aspects of the statistics of fields within the enclosure, but also accounts for the system-specific aspects introduced by the driving ports.

In this paper, we introduce such a model called the "random coupling model" (RCM) as it applies to enclosures filled with reciprocal media (generalization to enclosures filled with nonreciprocal media is straightforward [20], [21]). The foundation for a RCM treatment of statistical EM field properties is given in several previous publications [20]–[24]. Here, our objective is to develop the RCM into a quantitative prediction tool for the practical problem of calculating and mitigating the effects of EM interference within complicated metallic enclosures. In particular, we will provide an algorithm to predict the PDF of the voltages induced at specific components within an enclosure. We will experimentally validate and illustrate our approach using the example of a computer-box irradiated by continuous-wave (CW), short-wavelength EM energy. The primary requirement for the validity of our approach is that the typical length scale L (cube root of volume) of the enclosure be sufficiently large compared to the wavelength of the radiation λ_R (we expect the cavity will be sufficiently over moded when $L/\lambda_R \gtrapprox 3$).

This paper is divided into the following sections. In Section II, we briefly discuss the underlying principles of the RCM and present its salient features. Section III presents the general approach to calculating induced voltages in a system where the port has an arbitrary impedance. Section IV gives a brief overview of ways to determine the radiation impedance or admittance of an arbitrary port. In Section V, we present our experimental setup for the problem of EM coupling inside a computer box. Section VI then reports the experimental validation of the RCM induced voltage algorithm for this computer-box setup. Based on the insights gained, Section VII presents design guidelines for enclosures that make them more resistant to interference from an internal or external short-wavelength EM source. Section VIII then discusses the strengths, limitations, and caveats associated with using the RCM on realistic enclosures. Section IX concludes with a summary of the main points discussed in this paper. In Appendix A, we outline our algorithm to generate the universal impedance fluctuations for a given cavity or enclosure using random matrix theory.

II. Random Coupling Model

The RCM is formulated to address the problem of short-wavelength EM coupling into large, complicated metallic enclosures through multiple ports. This problem falls within a larger class of similar problems previously encountered in the fields of acoustics, quantum mesoscopic transport, and nuclear physics [25]. All these systems have short-wavelength waves (EM, acoustic or quantum mechanical) that are trapped within an irregularly shaped enclosure or potential well, in the case where the characteristic length of the system is substantially larger than the wavelength. In this limit, the waves within an enclosure can be approximated as rays that undergo specular reflections off the walls of the enclosure, much like the trajectory of a Newtonian point-particle elastically bouncing inside a similar-shaped enclosure. The dynamics of the rays within

the enclosure depend on the shape of the enclosing boundaries, and an enclosure is said to be "ray chaotic" if two typical rays launched with very slightly different initial conditions (slightly different initial location, or slightly different angular orientations) yield trajectories whose separation grows exponentially with distance along the ray during the time when this separation is small compared to the system size [26].

Ray chaos is common. Even very simple-shaped enclosures or cavities can produce chaotic ray dynamics [25], [27], [28]. The inherent complexities associated with the boundary shape of practical enclosures can easily create chaotic dynamics for the rays within the enclosure. In Section IV-A, we present a method to quantify the extreme sensitivity of wave properties to small perturbations.

A remarkable aspect of ray-chaotic systems is that despite their apparent complexity, they all possess certain universal statistical properties in their wave-scattering fluctuation characteristics [25], [29], and these statistical fluctuations are observed to be well described by the statistical properties of ensembles of large random matrices [30], [31]. Thus, it is possible to simulate the statistical wave-scattering behavior of ray-chaotic systems by using random matrix Monte Carlo techniques. For a ray-chaotic enclosure coupled to N_p ports, the RCM characterizes the fluctuations in the impedance and scattering matrices. The scattering matrix $\underline{\underline{S}}$ models the scattering region of interest in terms of a $N_p \times N_p$ complex-valued matrix. Specifically, it expresses the amplitudes of the N_p outgoing scattered waves $\underline{b}$ in terms of the N_p incoming waves $\underline{a}$ at the location of each port (i.e., $\underline{b} = \underline{\underline{S}}\ \underline{a}$). The impedance matrix $\underline{\underline{Z}}$ relates the complex voltages $\underline{V}$ at the N_p driving ports to the complex currents $\underline{I}$ at the N_p ports (i.e., $\underline{V} = \underline{\underline{Z}}\ \underline{I}$). The matrices $\underline{\underline{S}}$ and $\underline{\underline{Z}}$ are related through the bilinear transformation $\underline{\underline{S}} = [\underline{\underline{Z}_o}]^{1/2}(\underline{\underline{Z}} + \underline{\underline{Z}_o})^{-1}(\underline{\underline{Z}} - \underline{\underline{Z}_o})^{-1}[\underline{\underline{Z}_o}]^{-1/2}$, where $\underline{\underline{Z}_o}$ is a $N_p \times N_p$ real, diagonal matrix whose elements are the characteristic impedances of the transmission line input channels at the N_p driving ports.

It is convenient to think of modeling the statistical properties of the measured $N_p \times N_p$ impedance matrix $\underline{\underline{Z}}^{\rm cav}$ of the ray-chaotic enclosure as consisting of (see Fig. 1)—a "core" universal, detail-independent fluctuating part that we call the "normalized impedance matrix $\underline{\underline{\xi_Z}}$" ; and an "outer shell" imposed by the system-specific coupling details of the ports that is quantified by a radiation impedance matrix $\underline{\underline{Z}}^{\rm rad} = \underline{\underline{R}}^{\rm rad} + j{\rm Im}[\underline{\underline{Z}}^{\rm rad}]$ [21], where $\underline{\underline{R}}^{\rm rad}$ is known as the radiation resistance matrix. In terms of these quantities Zheng *et al*. [21] show that it is appropriate to model the impedance matrix $\underline{\underline{Z}}^{\rm cav}$ as follows:

$$\underline{\underline{Z}}^{\rm cav} = j{\rm Im}[\underline{\underline{Z}}^{\rm rad}] + [\underline{\underline{R}}^{\rm rad}]^{1/2}.\underline{\underline{\xi_Z}}.[\underline{\underline{R}}^{\rm rad}]^{1/2}. \qquad (1)$$

The radiation impedance matrix $\underline{\underline{Z}}^{\rm rad}$ is an experimentally accessible, $N_p \times N_p$ complex-valued matrix whose elements are nonstatistical, smoothly varying frequency-dependent quantities. The diagonal elements of $\underline{\underline{Z}}^{\rm rad}$ quantify the detail-specific aspects of the coupling between the ports and the enclosure for arbitrary port geometries. The off-diagonal elements represent the cross-talk between the different ports [21]. The radiation

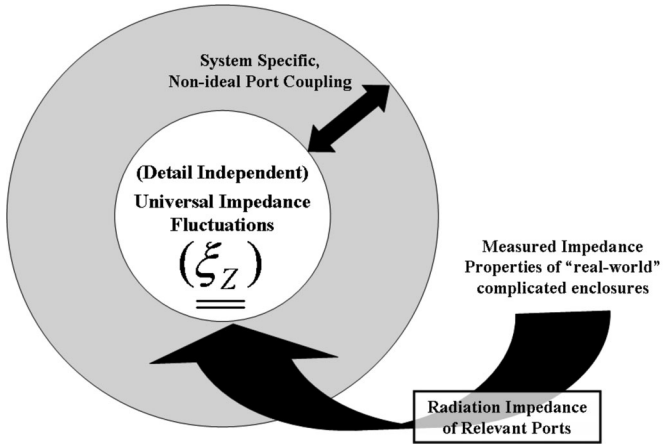

Fig. 1. Schematic showing a convenient way to visualize the RCM. The statistical properties of the measured impedance of wave-chaotic enclosures coupled to multiple ports consists of a detail independent, universally fluctuating normalized impedance $\underline{\underline{\xi_Z}}$, and the system-specific nonideal coupling details of the measurement ports. This nonideal port coupling is accurately quantified by the experimentally accessible and nonstatistical radiation impedance of the ports.

impedance matrix $\underline{\underline{Z}}^{\rm rad}$ can be visualized in the following way: if the enclosure whose impedance is represented by (1) is driven by the same ports (having the same coupling geometry) as before, but has the distant side walls of the enclosure and the internal scattering features moved out to infinity (or coated with a material that perfectly absorbs the incident waves), then the ports behave as a collection of free-space radiators. The boundary conditions corresponding to outgoing waves introduces a complex impedance matrix $\underline{\underline{Z}}^{\rm rad} = \underline{\underline{R}}^{\rm rad} + j{\rm Im}[\underline{\underline{Z}}^{\rm rad}]$ at the plane of measurement of the driving ports. This is illustrated schematically in Fig. 2 for an arbitrary enclosure coupled to two ports. The radiation resistance $\underline{\underline{R}}^{\rm rad}$ is a measure of the ability of the port to radiate energy to the far field, whereas ${\rm Im}[\underline{\underline{Z}}^{\rm rad}]$ is a measure of the reactive energy stored in the near field of the port [22].

The universally fluctuating quantity $\underline{\underline{\xi_Z}}$ corresponds to the impedance matrix of an enclosure that is "perfectly coupled" (as defined in Section I) to its driving ports. Mathematically, perfect coupling refers to the situation when $\underline{\underline{Z}}^{\rm rad} = \underline{\underline{Z_o}}$, where $\underline{\underline{Z_o}}$ is the diagonal matrix of characteristic impedances of transmission lines that connect to the ports. If $\underline{\underline{Z}}^{\rm rad}$ is known, (1) can be solved to determine the universal normalized impedance $\underline{\underline{\xi_Z}}$ in terms of measured impedance matrices $\underline{\underline{Z}}^{\rm cav}$ and $\underline{\underline{Z}}^{\rm rad}$

$$\underline{\underline{\xi_Z}} = [\underline{\underline{R}}^{\rm rad}]^{-1/2}.(\underline{\underline{Z}}^{\rm cav} - j{\rm Im}[\underline{\underline{Z}}^{\rm rad}]).[\underline{\underline{R}}^{\rm rad}]^{-1/2}. \qquad (2)$$

The normalized impedance matrix $\underline{\underline{\xi_Z}}$ corresponds to a normalized scattering matrix $\underline{\underline{\xi_S}} = (\underline{\underline{\xi_Z}} - \underline{\underline{I}}).(\underline{\underline{\xi_Z}} + \underline{\underline{I}})^{-1}$, and a normalized admittance matrix. Here, $\underline{\underline{I}}$ is the $N_p \times N_p$ identity matrix, and the superscript $^{-1}$ indicates a matrix-inversion operation.

According to the RCM, the only parameter on which the statistical properties of $\underline{\underline{\xi_Z}}, \underline{\underline{\xi_S}}$, or $\underline{\underline{\xi_Y}}$ depends is the dimensionless enclosure loss parameter α. The loss parameter is simply the

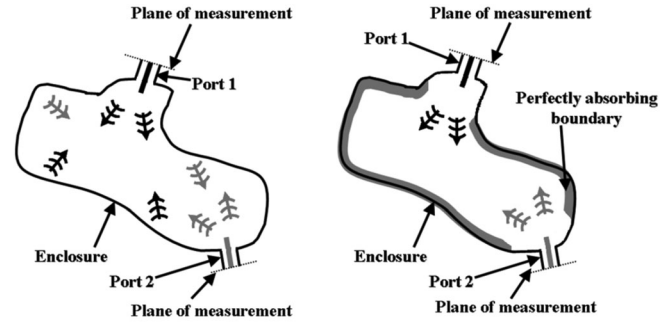

Fig. 2. (a) Schematic representation of a complicated enclosure coupled to two ports. The measured impedance of the enclosure $\underline{\underline{Z}}^{\mathrm{cav}}$ is a wildly fluctuating quantity on account of the waves originating from the two ports and experiencing multiple reflections before returning back to the ports. We refer to this condition as the "enclosure case." (b) Schematic representation of the complicated enclosure in (a) that is coupled to two ports that retain their coupling geometry, but have the distant sidewalls coated with a perfectly absorbing boundary. The measured impedance of this enclosure $\underline{\underline{Z}}^{\mathrm{rad}}$ is now a smoothly varying function of frequency and arises on account of the waves originating from the two ports and radiating outward without experiencing any internal reflections back to the ports. We refer to this condition as the "radiation case."

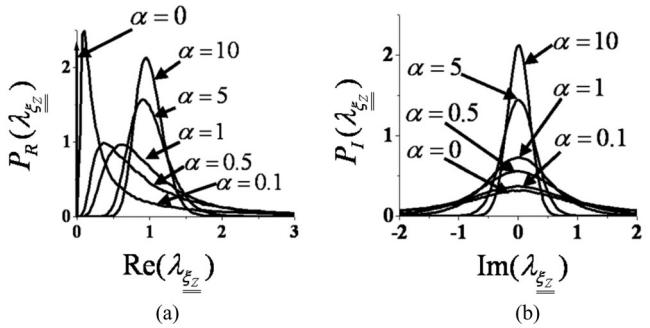

Fig. 3. RCM predictions for the marginal PDFs of the (a) real $\mathrm{Re}(\lambda_{\underline{\underline{\xi}}_Z})$ and (b) imaginary $\mathrm{Im}(\lambda_{\underline{\underline{\xi}}_Z})$ parts of the eigenvalues of $\underline{\underline{\xi}}_Z$ as a function of increasing loss parameter α, for a wave-chaotic enclosure filled with a medium having real, symmetric permittivity, and permeability tensors.

ratio of the 3-dB width of the resonant modes to the mean spacing in frequency between the modes. For a large 3-D vacuum-filled EM enclosure, $\alpha = k^3 V/(2\pi^2 Q)$, where $k = 2\pi f/c$ is the wavenumber for the wave of frequency f, and V represents the EM volume of the cavity. The quantity Q represents the typical loaded quality factor of the enclosure and is defined as the ratio of the EM energy stored to the power leaving the unexcited cavity (due to ohmic and dielectric losses, as well as power leaving through the ports) per cycle. The loss parameter α can range from 0 (for a loss-less enclosure) to ∞.

The eigenvalues of $\underline{\underline{\xi}}_Z$ are correlated and have a joint PDF that can be calculated from random matrix theory (see Appendix A). From such a distribution function, one can obtain marginal probability distributions for the real and imaginary parts of a single eigenvalue; we denote these marginal PDF's by $P_R(\lambda_{\underline{\underline{\xi}}_Z})$ and $P_I(\lambda_{\underline{\underline{\xi}}_Z})$.

For an enclosure, which is filled with a reciprocal medium having a real, symmetric permittivity, and permeability tensor, Fig. 3 shows the evolution of these marginal PDFs with increasing values of α [21], as calculated from random matrix theory. In the lossless case, $Q = \infty$ ($\alpha = 0$), and the eigenvalues of $\underline{\underline{\xi}}_Z$ are purely imaginary and $P_I(\lambda_{\underline{\underline{\xi}}_Z})$ is Lorentzian distributed with zero mean and unit full-width-at-half-maximum. As losses increase ($\alpha > 0$), $\underline{\underline{\xi}}_Z$ develops a nonzero real part, and $P_R(\lambda_{\underline{\underline{\xi}}_Z})$ evolves from being peaked near zero for low α toward being a Gaussian distribution that peaks at $\mathrm{Re}(\lambda_{\underline{\underline{\xi}}_Z}) = 1$ for large α [see Fig. 3(a)]. At the same time, $P_I(\lambda_{\underline{\underline{\xi}}_Z})$ loses its long tails (associated with the Lorentzian distribution at $\alpha = 0$) and begins to sharpen up, developing a Gaussian appearance at large α [see Fig. 3(b)]. For all values of α, the mean value of $\mathrm{Re}(\lambda_{\underline{\underline{\xi}}_Z})$ (denoted $\langle \mathrm{Re}(\lambda_{\underline{\underline{\xi}}_Z})\rangle$) is equal to 1 (see appendix of [20]), while the mean value of $\mathrm{Im}(\lambda_{\underline{\underline{\xi}}_Z})$ (denoted $\langle \mathrm{Im}(\lambda_{\underline{\underline{\xi}}_Z})\rangle$) is equal to 0. Approximate analytic expression for $P_R(\lambda_{\underline{\underline{\xi}}_Z})$ and $P_I(\lambda_{\underline{\underline{\xi}}_Z})$ for all values of α are given in [32]. For the results discussed in this paper, we will employ a random matrix Monte Carlo approach [33], [see Appendix A] to generate the theoretical RCM predictions for $P_R(\lambda_{\underline{\underline{\xi}}_Z})$ and $P_I(\lambda_{\underline{\underline{\xi}}_Z})$.

For $\alpha \gg 1$, [20] predicts that the variance of $P_R(\lambda_{\underline{\underline{\xi}}_Z})$ (denoted σ^2_{RZ}) is approximately equal to the variance of the marginal PDF of $P_I(\lambda_{\underline{\underline{\xi}}_Z})$ (denoted σ^2_{IZ}). The magnitudes of these variances depend only upon the value of the cavity loss parameter α and the presence of only reciprocal media, i.e

$$\sigma^2_{RZ} = \sigma^2_{IZ} \cong \frac{1}{\pi\alpha} \text{ for } \alpha \gg 1. \tag{3}$$

Equation (3) has been experimentally validated in [22] and [33] for $\alpha > 5$, and will be assumed to hold true for the results presented in this paper.

The existence of the universal fluctuations in the normalized impedance, scattering and admittance properties of one-port and two-port, quasi-2-D ray-chaotic enclosures has been experimentally validated [22]–[24], and shown to be in agreement with predictions of the RCM. A similar statistical EM wave model describing only the fluctuations in the impedance of large complicated one-port enclosures has been presented in [34] and [35]. This model uses the "terminal impedance" (similar in principle to the radiation impedance) of the port to quantify the nonideal port coupling over narrow frequency bands, and derives an expression similar to (1). The RCM, however, incorporates all the predictions of [34] and [35] and goes further to include complicated enclosures coupled to multiple ports over arbitrarily large frequency ranges. This aspect of RCM makes it possible to consider the induced voltage and current statistics inside complicated enclosures driven by multiple ports.

III. RCM Induced Voltage Calculation

In the case of a computer-box, high-frequency EM radiation can couple into the system through several independent channels (connectors, cooling vents, exposed wires, etc.). Also, internal components such as printed circuit board (PCB) tracks

and integrated circuits can emit their own EM radiation. All these channels setup complicated standing wave patterns within the metallic enclosure of the computer box. The RCM can be applied to this problem through two levels of abstraction. At the first level, we treat all relevant sources and sinks of radiation as "generalized ports." By "relevant" we mean those discrete components or features that are actively adding (or taking away) energy to (from) the system, which are classified as either source (target) ports, respectively. For instance, in the scenario of an external plane wave incident on a computer box, a relevant source port may be the cooling vent (aperture) that allows the plane-wave energy to couple into the box, while a target-port might be the PCB bus track (microstrip antenna) that carries the coupled energy to a sensitive IC chip. The problem of determining the radiation impedances of the relevant ports can be challenging. In the next section, we briefly summarize methods to determine the radiation impedance of relevant ports based on their physical geometries.

Unlike a regular microwave cavity resonator, where the ports tend to be at the interface between the external environment and the cavity resonator, here a generalized port can lie entirely within the confines of the cavity resonator. The presence of other components (memory cards, wire cables, etc.) within the computer box will be accounted for in the model through the scattering of the waves they produce within the enclosure, as well as modifications to the enclosure volume and quality factor Q. Once the relevant generalized ports have been identified, the second level of abstraction treats the computer box as a wave-chaotic enclosure with N_p ports, where N_p corresponds to the sum of all generalized ports. In what follows, we explain the framework of the RCM induced voltage algorithm taking the example of a computer box with two relevant generalized ports ($N_p = 2$) denoted as "port 1"(source) and "port 2"(target). Generalization to an arbitrary number of ports is straightforward. The algorithm essentially requires only three pieces of information in order to make accurate statistical predictions for the induced voltages at the target port for a specified CW excitation at port 1 (see Fig. 4). These three quantities are as follows.

1) The loss parameter α for the enclosure.
2) The 2×2 radiation-impedance matrix of the source and target ports within the enclosure at the frequencies of interest $\underline{\underline{Z}}^{\rm rad}(f)$. Since $\underline{\underline{Z}}^{\rm rad}(f)$ is a nonstatistical quantity, it can either be directly measured (as described in Section V), determined analytically, or determined numerically using conventional EM-solver software.
3) The frequency f dependence of the radiated power at the source port $\tilde{P}_1(f)$.

For a 3-D wave-chaotic enclosure, the loss parameter is $\alpha = k^3 V/(2\pi^2 Q)$. The value of α in turn dictates the shapes and scales of the normalized impedance matrix $\underline{\underline{\xi}}_Z$ element PDFs (see Fig. 3), which can be numerically generated using random matrix Monte Carlo simulations [33, Appendix A]. The numerically derived ensemble of normalized impedance $\underline{\underline{\xi}}_Z$ matrices can then be combined with the measured/calculated radiation-impedance matrix $\underline{\underline{Z}}^{\rm rad}$ and (1), to yield a numerical estimate of the PDF of the system-specific cavity-impedance

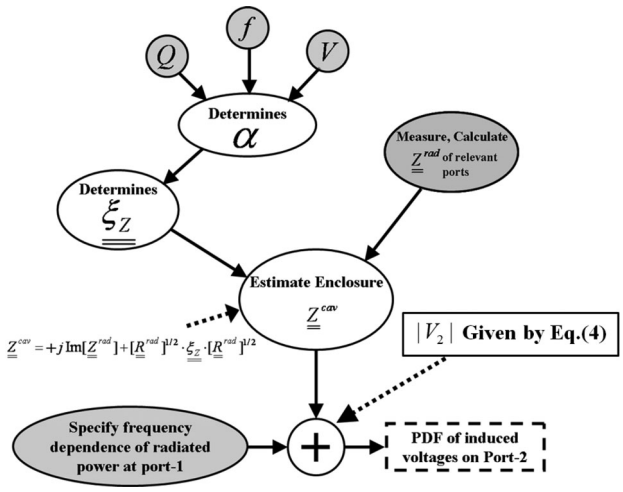

Fig. 4. Flowchart indicating the steps of the RCM induced voltage algorithm. The inputs to the RCM Voltage algorithm are the value of the loss parameter α, the radiation impedance matrix of source and target ports $\underline{\underline{Z}}^{\rm rad}$, and the frequency dependence of the radiated power at port 1 $\tilde{P}_1(f)$. The loss parameter α is dependent on the frequency f, enclosure volume V and typical enclosure quality-factor Q at frequency f.

matrix $\underline{\underline{Z}}^{\rm cav} = \begin{bmatrix} Z_{11}^{\rm cav} & Z_{12}^{\rm cav} \\ Z_{21}^{\rm cav} & Z_{22}^{\rm cav} \end{bmatrix}$ (see Fig. 4). Finally, using the 2×2 impedance matrix for a two-port microwave network [36], it is possible to determine the PDF of the magnitude of the induced voltage at a target port with impedance Z_L ($P_V(|V_2|)$) for the specified frequency dependence of the radiated power $\tilde{P}_1(f)$ at the source port through

$$|V_2| = \left| \sqrt{\frac{2\tilde{P}_1(f)|Z_p|^2 |Z_{11}^{\rm cav}|^2}{{\rm Re}|Z_{11}^{\rm cav}|}} \right| \tag{4}$$

where

$$Z_p = \frac{Z_{12}^{\rm cav} Z_L / Z_{\rm eq}}{Z_{22}^{\rm cav} + Z_L} \text{ and } Z_{\rm eq} = Z_{11}^{\rm cav} - \frac{Z_{12}^{\rm cav} Z_{12}^{\rm cav}}{Z_{22}^{\rm cav} + Z_L}. \tag{5}$$

In the limit where the load impedance approaches infinity (open-circuit on port 2), the induced voltage simplifies to

$$|V_2| = \left| \sqrt{\frac{2\tilde{P}_1(f)|Z_{21}^{\rm cav}|^2}{{\rm Re}|Z_{11}^{\rm cav}|}} \right|. \tag{6}$$

For this last expression, we assume port 2 to be open circuited so that the only voltage present on port 2 is induced by the excitation from port 1 and not influenced by any sources (or load impedances) that may be connected to port 2. We will use this limit in the calculated induced voltage distributions presented later.

IV. Estimating the Radiation Impedance and Admittance of Typical Coupling Structures

In this section, we briefly review the ways in which the impedance (or admittance) matrix is defined for a port, and then discuss how its values are determined analytically. We then consider alternative methods to estimate the radiation impedance/admittance matrix of complicated ports using computational EM codes, as well as through direct experiments. The

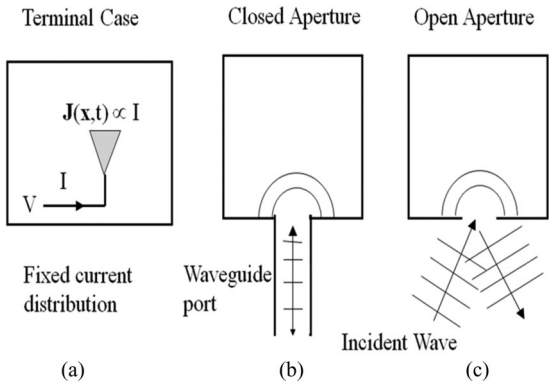

Fig. 5. Schematic diagram showing three typical coupling scenarios associated with practical use of the RCM. The three cases are (a) terminal, (b) closed-aperture, and (c) open-aperture coupling cases.

appropriate method to be adopted is in most cases dependent on the complexity of the radiating structure and other logistical factors such as experimental setup time. In the analytical approach, we identify three situations of interest, which we label the terminal case, the closed-aperture case, and the open-aperture case, as shown in Fig. 5. The precise definition of the impedance matrix will vary in these cases, as will the method of calculation of the matrix. However, all three of these cases can still be treated within the RCM.

A. Terminal Case

The terminal case [see Fig. 5(a)] applies to the situation where a port is excited through a single mode transmission line, and the excitation of the port can be prescribed by a single variable: the voltage, or current, or amplitude of the incident wave on the transmission line. Our studies of the excitation of cavities by signals on cables, as described in Section VI, are examples of this case. In addition, a terminal or lead on an integrated circuit can be treated as an example of this case if one considers the input to the circuit as a lumped element and the conductors and dielectric material surrounding the integrated circuit as an antenna. In the terminal case, determination of the radiation impedance becomes equivalent to solving for the fields surrounding an antenna that is driven by a transmission line. It is, thus, important to account for the geometry and dielectric properties of the material surrounding (within several wavelengths) the terminal. Calculation of the port impedance can be quite complicated as it involves the self-consistent determination of the current in all conductors and polarization of all dielectrics near the port. A simple case is that of an antenna that is small compared with a wavelength. In this case, the current distribution in the antenna is fixed. An example of this is that of a coaxial antenna in a 2-D cavity [20], [21]. Further details about calculating the radiation impedance in the terminal case can be found in [37].

B. Aperture Cases

The closed-aperture case [see Fig. 5(b)] applies to situations in which the cavity is excited through an aperture that is connected to a waveguide. In this case, the port is characterized by an impedance (or scattering) matrix that has a dimension equal to the number of modes used to represent the fields in the aperture. The open-aperture case [see Fig. 5(c)] applies when the aperture is illuminated by a plane wave incident with a wave vector $\mathbf{k}^{\mathrm{inc}}$ and polarization of magnetic field $\mathbf{H}^{\mathrm{inc}}$ that is perpendicular to $\mathbf{k}^{\mathrm{inc}}$. These cases are treated in detail by [37].

The analytic approach for estimating the radiation impedance of simple radiating structures has been used to estimate the radiation impedance of monopoles [38], short and long dipole radiators [34], [35], [39], horn antennas [40], and microstrip antennas [41]. However, when the internal geometry of the enclosure surrounding the port becomes more complicated, such as due to the presence of metal side walls or dielectric features in the near-field of the radiating ports, the analytic approximations can become too cumbersome to evaluate. In such cases, finite-element numerical-EM approaches based on time-domain or frequency-domain solvers can be utilized [42]. This numerical approach has proved to be successful for modeling aperture coupling within large enclosures such as automobiles [43] and computer boxes [44], [45]. Commercially available EM solver codes now have the ability to model very complex EM coupling scenarios, such as estimating the coupling between the pins of an IC chip [46], [47]. By using a combination of these numerical solver codes and the RCM, it is possible to come up with statistical descriptions for induced voltages on the pins of ICs for given excitation stimulus on an aperture-type cooling vent.

C. Experimental Determination of Radiation Impedance Matrix

Though powerful and reliable, numerical EM solver codes can sometimes be very expensive both in computational time and required hardware resources in order to obtain a sufficient degree of accuracy for the port radiation impedance quantities. A third approach to determining radiation impedance is based on direct experimental measurements and can, in some cases, be faster to set up and measure as compared to the numerical techniques. As reported in our experimental studies in Section VI, the experimental radiation impedance measurement consists of simulating an outward radiation boundary condition for the source and target ports by coating all the inner side walls and internal components in the far field of the ports with microwave/radar absorber. In some cases, where it might not be possible to experimentally create such an outward radiation boundary condition, an indirect experimental method may be adopted [48]. The accuracy of the experimentally measured radiation impedance is dictated by the frequency-dependent absorptive properties of the microwave/radar absorber used. Moreover, for short-wavelengths the coupling properties of the port are very sensitive to small changes in the port orientation. These factors can affect the repeatability and reliability of the experimentally measured radiation impedances.

As shown in Section VI of this paper, one can experimentally determine an approximate radiation impedance by taking an

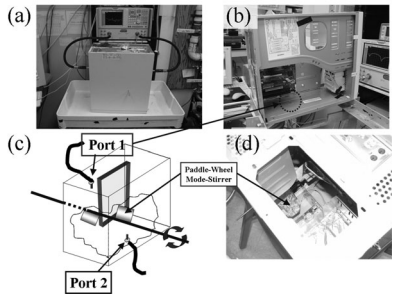

Fig. 6. (a) Photograph of the experimental setup of the computer box used for testing the RCM induced voltage algorithm. The computer box is connected to the Agilent E8364B vector network analyzer (in background). (b) Photograph of the computer box with the outer metallic-casing removed. The motherboard and one of the driving ports (port 1) on the bottom plate of the computer box cavity are visible. (c) Schematic showing the location of the two driving ports, and the paddle-wheel mode stirrer used to generate an ensemble of cavity measurements. (d) Photograph showing one of the paddle-wheel blades of the mode stirrer.

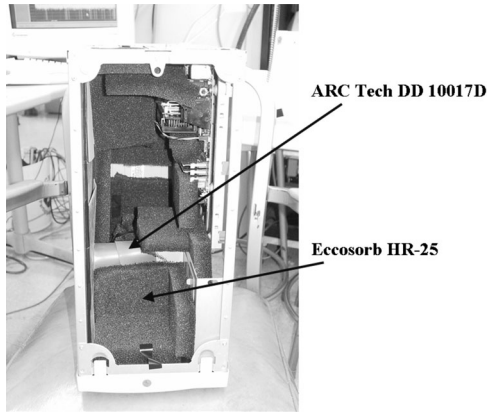

Fig. 7. Photograph of the experimental setup for the implementation of the radiation case. All inner side walls are coated with a dielectric absorber (ARC Tech DD 10017D), while the internal electronics are coated with a microwave foam absorber (Eccorsorb HR-25). A small circular region (about 8 cm in radius) around each driving port (not visible in photograph) is left uncoated to retain the near-field structure of the driving ports.

ensemble average of cavity impedances. This requires that the ensemble includes enough distinct realizations of the system to destroy the contributions of short orbits [49]–[51].

V. Experimental Setup

We have performed experiments to validate the RCM induced-voltage algorithm as described in Section III. The 3-D enclosure under study is a typical computer box of physical outer dimensions 38 cm $\times$ 21 cm $\times$ 23 cm see Fig. 6(a)], which contains all the internal electronics—motherboard, memory chips, network card, etc. [see Fig. 6(b)]. The floppy drive, CDROM-drive, and SMPS power-supply unit were removed to increase the internal volume of the enclosure and also to decrease the inherent enclosure loss. The enclosure was excited by means of two ports, labeled port 1 and port 2 in Fig. 6(c), located on the top and bottom walls of the box. We consider the frequency range of 4–20 GHz. The free-space wavelength at 4 GHz corresponds to about 7.5 cm that is about three times smaller than the smallest enclosure dimension. The ports are sections of coaxial transmission lines that act as dipole radiators with the exposed inner conductor of diameter 1.27 mm, extending 0.87 cm (for port 1) and 1.3 cm (for port 2) into the volume of the enclosure from the side walls.

To make a statistical analysis of the EM response of the computer-box enclosure, the first step involves measuring a large ensemble of the full 2×2 enclosure scattering matrix $\underline{\underline{S}}^{\rm cav} = \begin{bmatrix} S_{11}^{\rm cav} & S_{12}^{\rm cav} \\ S_{21}^{\rm cav} & S_{22}^{\rm cav} \end{bmatrix}$ using an Agilent E8364B vector network analyzer. This is referred to as the "enclosure case." To realize this large ensemble, a mode stirrer is introduced into the volume of the enclosure. The mode stirrer [shown in schematic in Fig. 6(c)] consists of a central metallic shaft (shown as the black line) of diameter 5 mm with two paddle-wheel-type blades (gray-colored rectangles) measuring approximately 10 cm $\times$ 5 cm and placed 7 cm apart. The two blades are made of cardboard paper coated with aluminum foil [see Fig. 6(d)] and are oriented perpendicular to each other on the shaft. Each orientation of the blades within the cavity results in a different internal field configuration. For each configuration, $\underline{\underline{S}}^{\rm cav}$ is measured as a function of frequency from 4 to 20 GHz in 16 000 equally spaced steps. By rotating the shaft through 20 different positions, an ensemble of 320 000 computer-box enclosure scattering matrices is, thus, collected. From the $S_{21}^{\rm cav}(\omega)$ measurements, it is inferred that the typical loaded-Q of the computer-box enclosure ranges from about 45 at 4 GHz to about 250 at 20 GHz.

The port radiation-impedance measurement involves simulating an outward radiation condition for the two driving ports, but retaining the coupling structure as in the "enclosure case." To achieve this condition, the mode stirrer is removed and all internal electronics and inner surfaces of the cavity side-walls are coated with microwave absorber—Eccosorb HR-25 and ARC-Tech DD10017D, respectively, which provides about 25 dB of reflection loss over the frequency range of the experiment (see Fig. 7). This is intended to minimize reflections within the computer-box enclosure. A circular area of about 8-cm radius is left uncoated around each of the ports so as to retain the near-field structure of the radiating ports. The "radiation case" now involves measuring the resultant 2×2 radiation-scattering matrix, $\underline{\underline{S}}^{\rm rad} = \begin{bmatrix} S_{11}^{\rm rad} & S_{12}^{\rm rad} \\ S_{21}^{\rm rad} & S_{22}^{\rm rad} \end{bmatrix}$, from 4 to 20 GHz with the same 16 000 frequency steps as in the "enclosure case." This is a single realization, deterministic (nonstatistical) measurement.

VI. Experimental Results

The objective of the current section is to experimentally show the applicability of the "RCM induced voltage algorithm" to address the practical problem of predicting induced voltage PDFs at specific target-ports within complicated enclosures, such as a computer box. To achieve this objective, we first need to establish three aspects of the EM wave scattering within the enclosure. First, we need to experimentally prove the existence of wave-chaotic scattering (see Section VI-A). Second, the applicability of the port radiation impedance (scattering) matrix to account for the frequency-dependent coupling in a 3-D

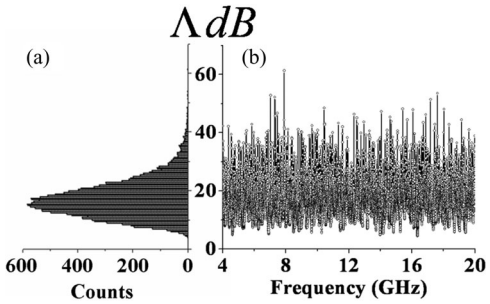

Fig. 8. (a) Histogram of the estimated ratio Λ of the maximum transmitted power to the minimum transmitted power at each frequency for the 20 different positions of the mode stirrer. The histogram has a mean of 17.3 dB and a standard deviation of 6.2 dB. (b) Variation in Λ with frequency (shown as the circles). A dynamic range of nearly 55 dB is observed for Λ over the frequency range of 4–20 GHz.

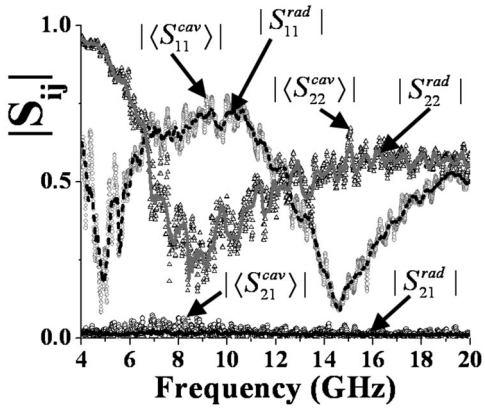

Fig. 9. Measured computer-box enclosure scattering matrix elements as a function of frequency. The circles, triangles, and pentagons represent the magnitude of the ensemble-averaged computer-box cavity $|\langle S_{11}^{\rm cav}\rangle|$, $|\langle S_{22}^{\rm cav}\rangle|$, and $|\langle S_{21}^{\rm cav}\rangle|$ elements, respectively. The dashed black line, solid gray line, and solid black line represent the magnitude of the measured radiation-scattering elements $|S_{11}^{\rm rad}|$, $|S_{22}^{\rm rad}|$ and $|S_{21}^{\rm rad}|$, respectively, which closely follow the general trend in the corresponding ensemble-averaged enclosure scattering matrix elements.

enclosure, where polarization of the waves and the effects of field variations associated with the presence of side walls has to be established experimentally (see Section VI-B). Third, the existence of universal fluctuations in the normalized impedance matrix for the computer-box enclosure has to be established and shown to be in agreement with corresponding predictions from RCM (see Section VI-C). Finally, in Section VI-D, we provide experimental results that validate the "RCM induced voltage algorithm" for the experimental setup discussed in Section V.

A. Establishing the Existence of "Wave-Chaos" Inside the Computer-Box Enclosure

In an enclosure, wave chaos manifests itself as extreme sensitivity of the internal field quantities to small changes in the wave frequency and in the enclosure's internal configuration. For the computer-box enclosure, this can be inferred by estimating the ratio of the maximum transmitted power to the minimum transmitted power at each frequency for the 20 different positions of the mode stirrer. This power ratio, denoted as $\Lambda = (\max(|S_{21}^{\rm cav}(f)|^2))/(\min(|S_{21}^{\rm cav}(f)|^2))$ (shown on a log scale in Fig. 8), has a distribution that is fairly wide with a mean of 17.3 dB and a standard deviation of 6.2 dB [see Fig. 8(a)]. The dynamic range of Λ is nearly 55 dB over the frequency range of 4–20 GHz [shown as the circles in Fig. 8(b)]. This indicates that there are significantly large field fluctuations within the computer-box enclosure as the mode stirrer is rotated, characteristic of wave-chaotic systems.

B. Characterizing the Nonideal Port Coupling Through the Measured Radiation Scattering Matrix

In Fig. 9, the average measured scattering matrix elements and the measured scattering matrix elements in the radiation case are shown as a function of frequency. The circles, triangles, and pentagons represent the magnitude of the ensemble-averaged computer-box "enclosure case" $|\langle S_{11}^{\rm cav}\rangle|$, $|\langle S_{22}^{\rm cav}\rangle|$, and $|\langle S_{21}^{\rm cav}\rangle|$ elements, respectively. The magnitude of the ensemble averaged scattering matrix elements is indicative of the degree of nonideal coupling between the ports and the cavity [52], [53].

A frequency range where the coupling between port i and the cavity is good results in small values of $|\langle S_{ii}^{\rm cav}\rangle|$ $(i = 1, 2)$. As can be seen in the figure, the two ports have rather different frequency-dependent coupling characteristics (indicated by the circles and triangles for port 1 and port 2, respectively). The dashed black line, solid gray line, and solid black lines represent the magnitude of the measured radiation-scattering elements $|S_{11}^{\rm rad}|$, $|S_{22}^{\rm rad}|$, and $|S_{21}^{\rm rad}|$, respectively, which closely follow the general trend of the respective ensemble averaged scattering elements over the entire frequency range. This indicates that the radiation scattering matrix (or equivalently the radiation impedance) elements accurately quantify the nonideal coupling between the ports and the computer-box enclosure at all frequencies. The slight oscillatory nature of the radiation-scattering matrix elements is attributed to imperfections in the absorber properties, allowing a small amount of wave energy to travel from a port to either itself or another port by following a path that reflects from the absorber [24], [49]–[51], [54], [55].

We can also use numerical methods to determine the radiation impedance matrix in this case. Fig. 10(a) shows a model of an aluminum box of dimensions 38 cm $\times$ 21 cm $\times$ 23 cm with the two side walls parallel to the *XZ* plane removed. The ports are modeled as sections of 50-Ω coaxial transmission lines with dimensions identical to that utilized in the experiment, i.e., dipole radiators with the exposed inner conductor of diameter 1.27 mm, extending 0.87 cm (for port 1) and 1.3 cm (for port 2) into the volume of the enclosure from the side walls. The relative spacing between the ports is also the same as in the experiment. The dashed black line, solid gray line, and solid black lines in Fig. 10(b) represent the magnitude of the numerically determined radiation-scattering elements $|S_{11}^{\rm rad}|$, $|S_{22}^{\rm rad}|$, and $|S_{21}^{\rm rad}|$, respectively, using CST Microwave Studio 2011. Note the similarity of the numerically determined radiation scattering elements to the corresponding experimentally measured quantities (see Fig. 9). In Fig. 10(c), all the side walls of the aluminum box model are removed, except for a region 8-cm square around

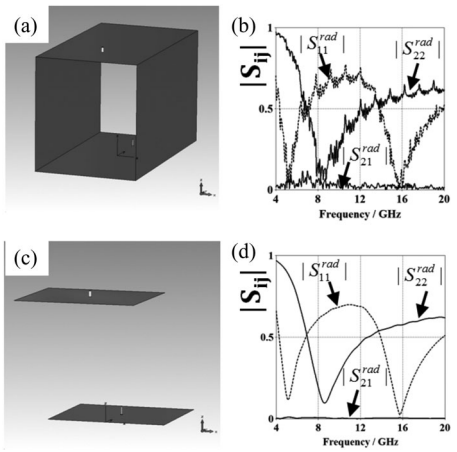

Fig. 10. (a) CST Microwave Studio model of an aluminum box of dimensions 38 cm × 21 cm × 23 cm with the sidewalls parallel to the *XZ* plane removed. The two ports are visible on the top and bottom plates of the box. (b) Dashed black line, solid gray line, and solid black line represent the magnitude of the calculated radiation-scattering elements $|S_{11}^{\rm rad}|$, $|S_{22}^{\rm rad}|$, and $|S_{21}^{\rm rad}|$, respectively. (c) CST Microwave Studio model of an aluminum box of dimensions 38 cm × 21 cm × 23 cm with all the side-walls removed, except for a region 8-cm square around the two ports. (d) Dashed black line, solid gray line, and solid black line represent the magnitude of the calculated radiation-scattering elements $|S_{11}^{\rm rad}|$, $|S_{22}^{\rm rad}|$, and $|S_{21}^{\rm rad}|$, respectively.

the two ports. The dashed black line, solid gray line, and solid black lines in Fig. 10(d) show the corresponding numerically estimated radiation-scattering elements $|S_{11}^{\rm rad}|$, $|S_{22}^{\rm rad}|$, and $|S_{21}^{\rm rad}|$, respectively. Note that the oscillatory nature of the radiation-scattering matrix elements arising from the reflections off the side walls is now eliminated.

These numerical results suggest a new experimental method to determine the radiation impedance matrix. One can create a port configuration like that shown in Fig. 10(c) in an anechoic chamber, and measurement of $\underline{\underline{S}}^{\rm rad}$ is straightforward. This method has been successfully employed for a 1 m^3 complex enclosure [56].

C. Establishing the Existence of Universal Impedance PDFs for the Computer-Box Enclosure

Having measured the ensemble of computer-box enclosure scattering matrices $\underline{\underline{S}}^{\rm cav}$, and the corresponding radiation-scattering matrix $\underline{\underline{S}}^{\rm rad}$ from Section IV, we convert these quantities into the corresponding enclosure impedance matrices $\underline{\underline{Z}}^{\rm cav}$ and radiation-impedance matrices $\underline{\underline{Z}}^{\rm rad}$, respectively using

$$\underline{\underline{Z}}^{\rm cav} = [\underline{\underline{Z_o}}]^{1/2}.(\underline{\underline{I}} + \underline{\underline{S}}^{\rm cav}).(\underline{\underline{I}} - \underline{\underline{S}}^{\rm cav})^{-1}.[\underline{\underline{Z_o}}]^{1/2} \quad \text{and}$$
$$\underline{\underline{Z}}^{\rm rad} = [\underline{\underline{Z_o}}]^{1/2}.(\underline{\underline{I}} + \underline{\underline{S}}^{\rm rad}).(\underline{\underline{I}} - \underline{\underline{S}}^{\rm rad})^{-1}.[\underline{\underline{Z_o}}]^{1/2} \qquad (7)$$

where the matrix $\underline{\underline{Z_o}}$ is a real diagonal matrix whose elements are the characteristic impedances of the transmission lines connected to the driving ports. Here, each port has a single operating mode with characteristic impedance of 50 Ω over the frequency range of the experiment. Each $\underline{\underline{Z}}^{\rm cav}$ is then normalized with the corresponding measured $\underline{\underline{Z}}^{\rm rad}$ at the same frequency to obtain the normalized impedance matrix $\underline{\underline{\xi_Z}}$ using (2).

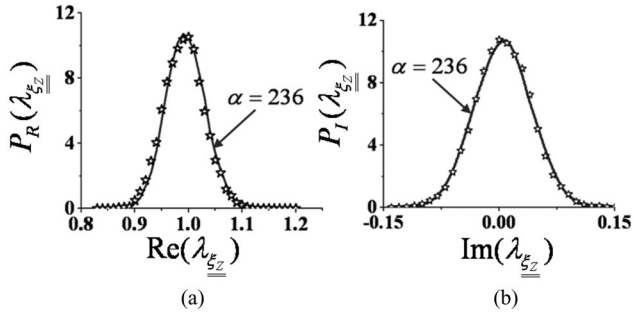

Fig. 11. Marginal PDFs for the (a) real and (b) imaginary parts of the grouped eigenvalues of the normalized computer-box enclosure impedance $\underline{\underline{\xi_Z}}$ (stars) in the frequency range of 17–18 GHz. Also shown are the single parameter, simultaneous fits for both the real and imaginary normalized impedance PDFs (solid lines), where the loss parameter $\alpha(\alpha = 236)$ is obtained from the variance of the data represented by the stars in (a) and (b).

We consider the experimentally determined normalized impedance $\underline{\underline{\xi_Z}}$ matrices that lie within the arbitrarily chosen frequency range of 17–18 GHz (where the loss parameter is roughly constant), which is defined as a "dataset." Each $\underline{\underline{\xi_Z}}$ matrix in our measured ensemble yields two complex eigenvalues. Thus, if there are $X_{\rm num}$ matrices in the ensemble, there are $2X_{\rm num}$ eigenvalues in the measured ensemble, which are placed together into a list. We have observed that using both eigenvalues in the list, as opposed to randomly considering one of the two eigenvalues, does not alter the statistical results that follow. Histogram approximations to the PDFs of the real $\mathrm{Re}(\lambda_{\underline{\underline{\xi_Z}}})$ and imaginary $\mathrm{Im}(\lambda_{\underline{\underline{\xi_Z}}})$ parts of the eigenvalues of $\underline{\underline{\xi_Z}}$ appearing on the list are shown in Fig. 11(a) and (b), respectively, by the star symbols. The variances σ^2 of experimental PDFs in Fig. 11(a) and (b) are nearly identical in magnitude, i.e., $(\sigma_{RZ}^2 \cong \sigma_{IZ}^2 = 1.35 \times 10^{-3})$. From the variance of the PDFs of the real $\mathrm{Re}(\lambda_{\underline{\underline{\xi_Z}}})$ and imaginary $\mathrm{Im}(\lambda_{\underline{\underline{\xi_Z}}})$ parts of the eigenvalues of $\underline{\underline{\xi_Z}}$ and by using (3), we estimate a value of the cavity loss parameter α for this dataset to be $\alpha \cong 236$. Using the value of $\alpha = 236$, a random matrix Monte Carlo simulation [Appendix A] yields the black curves shown in Fig. 11(a) and (b) for the real and imaginary parts of $\underline{\underline{\xi_Z}}$ PDFs i.e., $P_R(\lambda_{\underline{\underline{\xi_Z}}})$ and $P_I(\lambda_{\underline{\underline{\xi_Z}}})$, respectively. Good agreement is observed between the experimentally derived PDFs and those generated numerically from random matrix Monte Carlo simulations. This agreement also extends to the other 30 constant-α "datasets" examined over the frequency range of 4–20 GHz, and supports the existence of universal fluctuations in $\underline{\underline{\xi_Z}}$ for the computer-box enclosure.

D. Validity of the RCM Induced Voltage Algorithm for the Computer-Box Enclosure

To test the validity of the RCM induced voltage algorithm for the computer-box enclosure, we first chose an arbitrary frequency range of 4.5–5.5 GHz and assume that the losses do not change significantly in this range (i.e., α is approximately constant). From the $S_{21}^{\rm cav}(\omega)$ measurements, the typical Q for the computer-box cavity over this frequency range is estimated to be about 45 (i.e., $Q \cong 45$). An estimate of the

value of $\alpha = k^3V/(2\pi^2Q)$ using $k = 2\pi f/c$ with $f = 5$ GHz and $V = 0.38 \times 0.21 \times 0.23\,\mathrm{m}^3$ (the physical volume of the computer-box cavity), yields $\alpha \approx 24$. (Other methods to determine α are discussed in Appendix B of [33].) Note that since the computer-box enclosure contains components of different dielectric constants (such as the $FR-4$ material used to fabricate the motherboard), the EM-volume of the computer-box enclosure is different from the physical volume. However, since the computer-box enclosure is sufficiently lossy ($\alpha \gg 1$), the statistics of the normalized impedance are relatively insensitive to small changes in α. This mitigates the effect of errors in the estimate of the enclosure volume.

We then use random matrix Monte Carlo simulations [Appendix A] to generate an ensemble of 100 000 normalized impedance $\underline{\underline{\xi_Z}}$ matrices that correspond to a value of $\alpha = 24$. Combining this ensemble of $\underline{\underline{\xi_Z}}$ matrices with the measured 2×2 radiation impedance matrix $\underline{\underline{Z}}^{\mathrm{rad}}$ over the frequency range of 4.5–5.5 GHz using (1), an estimate for the ensemble of the computer-box enclosure impedances in the "enclosure case" is obtained. In order to determine the nature of the induced voltage PDFs at port 2, two scenarios are simulated by assuming two different functional forms for the frequency dependence of the radiated power at port 1.

1) A "flat-top" ($(\tilde{P}_1(\tilde{f}) = 1$)Watt) functional form for the port 1 power, radiated uniformly over the frequency range from 4.5 to 5.5 GHz [see inset of Fig. 12(a)].
2) A Gaussian-shaped ($(\tilde{P}_1(\tilde{f}) = e^{(\tilde{f}-\mu)^2/2\sigma^2}$)Watt) functional form for the port-1 radiated power defined over the frequency range from 4.5 to 5.5 GHz, which is centered at $\mu = 5$ GHz and $\sigma = \sqrt{0.025}$ GHz [see inset of Fig. 12(b)].

Note: In scenarios (1) and (2), we have assumed that the frequency-dependent port-1 radiated power is a purely real, scalar quantity. This assumption neglects any phase correlations between the frequency components of the radiated signal from port 1. We shall also assume that port 2 presents an open-circuit boundary condition [$Z_L = \infty$ in (4)].

The predicted PDF of the magnitude of the induced voltage at port 2 is shown as the black curve in Fig. 12(a) for the "flat-top" port-1 radiated power of scenario (1). The black curve in Fig. 12(b) represents the predicted PDF of the magnitude of the induced voltage at port 2 for the Gaussian-shaped port-1 radiated power of scenario (2). Note that the induced voltage PDFs in the two scenarios are rather different.

The stars in Fig. 12(a) represent the PDF of the induced voltage at port 2 for the "flat-top" port-1 radiated power of scenario (1) shown in inset and (6), where the terms Z_{11}^{cav} and Z_{21}^{cav} in (6) correspond to the experimentally measured enclosure-case impedances of the computer box. Similarly, the circles in Fig. 12(b) represent the PDF of the induced voltage at port 2 for the Gaussian-shaped port-1 radiated power of scenario (2) shown in inset and (6), where the terms Z_{11}^{cav} and Z_{21}^{cav} in (6) correspond to experimentally measured enclosure-case impedances of the computer box. Good agreement is found between the induced voltage PDFs that were determined numerically (black curves) using only the measured radiation impedance matrix and random matrix Monte Carlo simulations based upon a calculated value of α; and those induced voltage PDFs (symbols) that were generated using the experimentally measured enclosure-case impedance matrix ensemble. Similar agreement was seen in other frequency windows in the 4–20 GHz that we examined. This confirms the validity of the RCM voltage algorithm as an accurate and computationally fast method to predict the statistical nature of induced voltages at a given target port for a specified excitation at a source port.

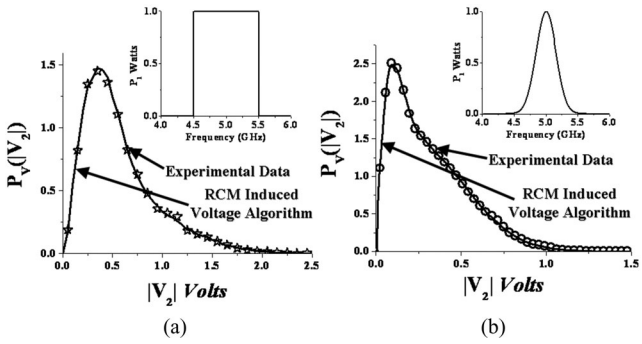

Fig. 12. (a) Numerically determined PDF of induced voltages at port 2 obtained using the RCM induced voltage algorithm for a "flat-top" functional form of the radiated power from port 1 (inset) is shown as the black curve. The black stars represent the experimentally derived PDF of induced voltages at port 2 obtained using the elements of the measured enclosure impedance matrix and (6), for the "flat-top" functional form of the radiated power from port 1 (inset). (b) Numerically determined PDF of induced voltages at port 2 obtained using the RCM induced voltage algorithm for a Gaussian-shaped frequency dependence of the radiated power from port 1 (inset) is shown as the black curve. The black stars represent the experimentally derived PDF of induced voltages at port 2 obtained using the elements of the measured enclosure impedance matrix and (6), for a Gaussian-shaped frequency dependence of the radiated-power from port 1 (inset). In all cases it is assumed that port 2 has open-circuit boundary conditions.

VII. Design Guidelines for Upset-Resistant Generic Enclosures

Based on the RCM, we can now make suggestions for design of systems that reduce the susceptibility to EM upset. Some simple design guidelines for generic complicated enclosures that can be useful in considerations of resilience to upset by an external (or internal) short-wavelength EM source are as follows.

1) *Increasing the value of the enclosure loss parameter* α: For a 3-D enclosure, $\alpha = k^3V/(2\pi^2Q)$. Increasing the value of α (e.g., by decreasing the quality factor Q by resistive loading such as the use of carbon-based microwave absorbers) decreases the fluctuations in the enclosure impedance values [14], [55]. The narrowing of the distributions with increasing α in Fig. 3 is a manifestation of this effect. This in turn reduces the probability for large internal field fluctuations, or equivalently large induced voltage fluctuations, on the components housed within the enclosure.
2) *Radiation impedance engineering*: As discussed in Section IV, perfect coupling implies $\underline{\underline{Z}}^{\mathrm{rad}} = \underline{\underline{Z}}_o$. Thus, creating a large impedance mismatch between the radiation impedance of the port and the characteristic

impedance of the transmission lines connected to that port will result in very poor transfer of the incoming EM energy into the interior of the cavity enclosure through the port. Apertures, cables, antennas, etc., can be engineered to have a large radiation impedance mismatch at the frequencies of concern. Section IV outlines how the radiation impedance can be calculated in general, and the RCM gives a quantitative description of the effectiveness of port mismatch on modifying the induced-voltage distribution. A detailed discussion of how to calculate the port radiation impedance for a large variety of ports is presented in [37].

3) *Use of nonreciprocal media*: The use of nonreciprocal media such as magnetized ferrites placed within a cavity enclosure can significantly decrease the amplitude of field intensities [20], [21], [57]. In addition to being inherently lossy (thereby increasing the α-value of the cavity enclosure), nonreciprocal media restrict instances of constructive interference between the rays bouncing within the cavity enclosure. This in turn reduces the formation of "hot spots" (regions of high EM field intensities) [57] within the cavity enclosure.

VIII. Assumptions, Caveats, and Future Work

The applicability of RCM is based on certain fundamental assumptions. First, the enclosure has to be substantially large compared to the wavelength of the EM radiation. This assumption translates into the enclosure supporting many EM modes below the lowest frequency of interest. Second, the enclosure has to display chaotic ray trajectories. Though this is generally a valid assumption, given the complexity of the internal details in most real-world enclosures such as computer boxes or aircraft fuselages, we note that some enclosures may show a mixture of chaotic and nonchaotic ray dynamics [25]. Such mixed dynamics are common in complicated enclosures that have several flat metallic surfaces facing each other. Under such conditions, the predictions of RCM may only be partially correct. The presence of flat surfaces within enclosures may also result in "scars" [58]–[60], which are modal patterns that exhibit large field intensities near closed ray trajectories. The presence of scars violates the random plane wave hypothesis within the enclosure, and is currently not treated by the RCM.

The RCM uses the radiation impedance matrix to quantify the nonideal and frequency-dependent coupling between the ports and the enclosure. It has been observed that in the limit where the number of statistically independent matrices in the ensemble for the enclosure impedance $\underline{\underline{Z}}^{\mathrm{cav}}$ is infinitely large, the mean value of $\underline{\underline{Z}}^{\mathrm{cav}}$ approaches $\underline{\underline{Z}}^{\mathrm{rad}}$, i.e., $\langle \underline{\underline{Z}}^{\mathrm{cav}} \rangle = \underline{\underline{Z}}^{\mathrm{rad}}$ (or equivalently, $\langle \underline{\underline{S}}^{\mathrm{cav}} \rangle = \underline{\underline{S}}^{\mathrm{rad}}$) [33], [55], [56], [61]. This observation is of great practical significance in realistic situations where it may not always be possible to accurately determine $\underline{\underline{Z}}^{\mathrm{rad}}$ either numerically or through experimental measurement.

The RCM has shown that besides the radiation impedance matrix of the relevant ports, the quantity that determines the shapes and scales of the fluctuations within the enclosure is the loss parameter $\alpha = k^3 V/(2\pi^2 Q)$. We note that in over-moded enclosures, the Q of the enclosure is frequency dependent and varies from mode to mode due to the slight differences in the modal patterns near the dissipative structures. However, this variation in Q from mode to mode is small (about 10%) [16] for suitably irregular complicated enclosures. Moreover, most realistic enclosures such as computer boxes, aircraft fuselages, or missile casings tend to be of relatively low Q (tens to hundreds). In such cases, the predicted PDFs of the enclosure impedance and scattering quantities are not very sensitive to the loss parameter α. Thus, a reasonable estimate of the average Q of the modes around the frequency of interest would suffice in most cases. One possible extension to RCM would be to include the variation of the loss parameter as a function of frequency. This would be useful when considering complicated enclosures irradiated by wide-band short-wavelength EM radiation.

Some other caveats about the RCM deserve mention. The RCM is a statistical frequency-domain model and should not be used to predict the outcome of a specific measurement for a specific situation. One should not use the RCM when the enclosure $Q \simeq 1$, or less. In this case there is no reverberation, and the basic assumptions of the model are not satisfied.

Treatment of time-varying and nonlinear loads attached to ports is presently beyond the capabilities of the frequency-domain RCM induced voltage algorithm and deserves further investigation. Other extensions of the RCM include treatment of transient input waveforms, and treatment of the phases of a broadband signal. Extending the RCM to include nonreciprocal wave propagation is straightforward and has already been outlined [20], [21]. It is also of interest to examine how the RCM breaks down in the limit of low frequency as the wavelength becomes comparable to the characteristic dimension of the enclosure.

The RCM can also be extended to explicitly include short orbits involving the ports. Short orbits are classical ray trajectories that start from a given port, bounce a small number of times, and then return to the same port, or go on to another port. Effects of these orbits are seen as systematic (nonstatistical) variations of the impedance matrix elements as a function of frequency. The RCM has recently been extended to include such orbits [49]–[51], [56].

The RCM can be generalized to a network of many interconnected complicated enclosures. The PDF of induced voltages on a port in a particular enclosure stimulated by a port in another enclosure can be estimated in the limit of weak coupling between the enclosures [62]. Using random matrix theory (RMT) and the random plane wave hypothesis, one can also calculate the statistical properties of loss in enclosures that are coupled by means of tunneling (e.g., coupling through an aperture beyond cutoff) [63].

IX. Conclusion

The results discussed in this paper provide experimental evidence in support of the utility of the RCM for statistically modeling short-wavelength EM wave scattering within 3-D complicated enclosures, coupled to multiple ports. The experimental results have shown that the radiation impedance matrix is extremely robust in quantifying the nonideal port coupling, even

when polarization of the waves and field fluctuations due to the presence of side walls in the near-field proximity of the driving ports plays a role. We have shown that a minimal amount of information (frequency, volume of the enclosure, typical Q of the enclosure, radiation impedance of the relevant ports, and an estimate of the frequency dependence of the radiated power at the source port) is needed to accurately predict the shape and scales of the induced voltages at specific target ports within large complicated enclosures. Based on the RCM, we have also suggested design guidelines to make a generic 3-D complicated enclosure (such as a computer box or aircraft fuselage) more resistant to upset from an external short-wavelength EM source.

APPENDIX A

For a wave-chaotic cavity enclosure filled with reciprocal media and coupled to N single-moded driving ports ($N \geqslant 1$), the $N \times N$ normalized impedance matrix $\underline{\underline{\xi_Z}}$ can be written as

$$\underline{\underline{\xi_Z}} = \frac{-j}{\pi}\underline{\underline{W}}\frac{1}{\underline{\underline{\lambda_Z}} - j\alpha\underline{\underline{I}}}\underline{\underline{W}}^T \tag{A.1}$$

where the matrix $\underline{\underline{W}}$ is an $N \times M$ coupling matrix with each element W_{nm} representing the coupling between the nth driving port ($1 \leqslant n \leqslant N$) and the mth eigenmode of the closed cavity ($1 \leqslant m \leqslant M$ and $M \gg N \geqslant 1$). Each W_{nm} is assumed to be an independent Gaussian-distributed random number of zero mean and unit variance. The matrix $\underline{\underline{W}}^T$ corresponds to the transpose of matrix $\underline{\underline{W}}$, and $\underline{\underline{I}}$ is a $M \times M$ identity matrix. The scalar quantity α corresponds to the enclosure loss parameter and $j = \sqrt{-1}$.

In order to obtain the matrix $\underline{\underline{\lambda_Z}}$, which is an $M \times M$ diagonal matrix with a set of M-values the following procedure is adopted. A real symmetric matrix $\bar{H}$ of size $5M \times 5M$ is generated whose elements are independent identically distributed with the on-diagonal elements chosen from a Gaussian distribution of zero-mean and unit-variance, and the off-diagonal elements chosen from a Gaussian distribution of zero mean and a variance of 0.5. For large M ($M \geqslant 200$ for the results discussed in this paper), the eigenvalues λ_M of $\bar{H}$ have nonuniform spacing and are distributed as per Wigner's "semicircle law" [30] with an average spacing for eigenvalues around the eigenvalue λ given by, $\Delta(\lambda) = \pi/(\sqrt{10M - \lambda^2}$. From this semicircle distribution, the middle M values are selected and then normalized by multiplying them with $\sqrt{10M}/\pi$, in order to create a sequence of normalized eigenvalues $\tilde{\lambda}_M$ with an approximately average spacing of unity.

The procedure outlined previous results in a single instance of the normalized impedance matrix $\underline{\underline{\xi_Z}}$. By repeating this procedure $100\,000$ times, a sufficiently large ensemble of $\underline{\underline{\xi_Z}}$ is generated from which its statistical descriptions (PDFs and its moments) are determined.

ACKNOWLEDGMENT

The authors would like to thank Dr. M. Harrison, Dr. J. Gaudet, and Dr. J. Rodgers, for useful discussions, and would like to thank referees for useful suggestions.

REFERENCES

[1] A. Kaya, L. Greenstein, and W. Trappe, "Characterizing indoor wireless channels via ray tracing combined with stochastic modeling," *IEEE Trans. Wireless Commun.*, vol. 8, no. 8, pp. 4165–4175, Aug. 2009.

[2] M. Jafri, J. Ely, and L. Vahala, "Graphical and statistical analysis of airplane passenger cabin RF coupling paths to avionics," in *Proc. 22nd Digital Avion. Syst. Conf.*, Oct. 2003, vol. 2, pp. 11.E.4–111–15.

[3] D. Johnson, M. Hatfield, and G. Preyer, "RF coupling measurements on passenger aircraft avionics exposed to cavity-mode excitation," in *Proc. 14th Digital Avion. Syst. Conf.*, Nov. 1995, pp. 427–432.

[4] C. Birtcher, S. Georgakopoulos, and C. Balanis, "In-flight EMI from portable electronic devices (PEDS): FDTD predictions vs. measurements," in *Proc. IEEE Antennas Propag. Soc. Int. Symp.*, vol. 2, pp. 686–689.

[5] M. Abrams, "Dawn of the e-bomb," *IEEE Spectrum*, vol. 40, no. 11, pp. 24–30, Nov. 2003.

[6] P. E. Nielsen, *Effects of Directed Energy Weapons [Electronic Resource]*. Washington, DC: NDU Press, 1994.

[7] J.-P. Parmantier, "Numerical coupling models for complex systems and results," *IEEE Trans. Electromagn. Compat.*, vol. 46, no. 3, pp. 359–367, Aug. 2004.

[8] R. Holland and R. S. John, *Statistical Electromagnetics*. New York: Taylor & Francis, 1999.

[9] S. W. McDonald and A. N. Kaufman, "Spectrum and eigenfunctions for a hamiltonian with stochastic trajectories," *Phys. Rev. Lett.*, vol. 42, no. 18, pp. 1189–1191, Apr. 1979.

[10] T. Lehman, "A statistical theory of electromagnetic fields in complex cavities," USAF Phillips Laboratory, Interaction Notes, Note 494, May 1993.

[11] P. Corona, G. Latmiral, and E. Paolini, "Performance and analysis of a reverberating enclosure with variable geometry," *IEEE Trans. Electromagn. Compat.*, vol. EMC-22, no. 1, pp. 2–5, Feb. 1980.

[12] R. H. Price, H. T. Davis, and E. P. Wenaas, "Determination of the statistical distribution of electromagnetic-field amplitudes in complex cavities," *Phys. Rev. E*, vol. 48, no. 6, pp. 4716–4729, Dec. 1993.

[13] D. Hill, "Electronic mode stirring for reverberation chambers," *IEEE Trans. Electromagn. Compat.*, vol. 36, no. 4, pp. 294–299, Nov. 1994.

[14] D. A. Hill, "Plane wave integral representation for fields in reverberation chambers," *IEEE Trans. Electromagn. Compat.*, vol. 40, no. 3, pp. 209–217, Aug. 1998.

[15] L. Cappetta, M. Feo, V. Fiumara, V. Pierro, and M. Pinto, "Electromagnetic chaos in mode-stirred reverberation enclosures," *IEEE Trans. Electromagn. Compat.*, vol. 40, no. 3, pp. 185–192, Aug. 1998.

[16] J. Barthélemy, O. Legrand and F. Mortessagne, "Inhomogeneous resonance broadening and statistics of complex wave functions in a chaotic microwave cavity," *Europhys. Lett.*, vol. 70, no. 2, pp. 162–168, 2005.

[17] G. Freyer, M. Hatfield, D. Johnson, and M. Slocum, "Comparison of measured and theoretical statistical parameters of complex cavities," in *Proc. IEEE Int. Symp. Electromagn. Compat. Symp. Record*, Aug. 1996, pp. 250–253.

[18] P. Corona, J. Ladbury, and G. Latmiral, "Reverberation-chamber research-then and now: A review of early work and comparison with current understanding," *IEEE Trans. Electromagn. Compat.*, vol. 44, no. 1, pp. 87–94, Feb. 2002.

[19] P. Corona, G. Ferrara, and M. Migliaccio, "Reverberating chambers as sources of stochastic electromagnetic fields," *IEEE Trans. Electromagn. Compat.*, vol. 38, no. 3, pp. 348–356, Aug. 1996.

[20] X. Zheng, T. M. Antonsen, and E. Ott, "Statistics of impedance and scattering matrices in chaotic microwave cavities: Single channel case," *Electromagnetics*, vol. 26, pp. 3–35, 2006.

[21] X. Zheng, T. M. Antonsen, and E. Ott, "The statistics of impedance and scattering matrices of chaotic microwave cavities with multiple ports," *Electromagnetics*, vol. 26, pp. 37–55, 2006.

[22] S. Hemmady, X. Zheng, E. Ott, T. M. Antonsen, and S. M. Anlage, "Universal impedance fluctuations in wave chaotic systems," *Phys. Rev. Lett.*, vol. 94, no. 1, p. 014102, 2004.

[23] S. Hemmady, X. Zheng, T. M. Antonsen, E. Ott, and S. M. Anlage, "Universal statistics of the scattering coefficient of chaotic microwave cavities," *Phys. Rev. E*, vol. 71, no. 5, p. 10, 2005.
[24] S. Hemmady, X. Zheng, J. Hart, T. M. Antonsen, E. Ott, and S. M. Anlage, "Universal properties of 2-port scattering, impedance and admittance matrices of wave chaotic systems," *Phys. Rev. E—Statist., Nonlinear Soft Matter Phys.*, vol. 74, no. 3, Pt 2, p. 036213, 2006.
[25] H.-J. Stöckmann, *Quantum Chaos: An Introduction*. Cambridge, U.K.: Cambridge Univ. Press, 1999.
[26] E. Ott, *Chaos in Dynamical Systems,* vol. 79. Cambridge, U.K. Cambridge Univ. Press, 1993, no. 484.
[27] V. Galdi, I. Pinto, and L. Felsen, "Wave propagation in ray-chaotic enclosures: Paradigms, oddities and examples," *IEEE Antennas Propag. Mag.*, vol. 47, no. 1, pp. 62–81, Feb. 2005.
[28] V. Fiumara, V. Galdi, V. Pierro, and I. Pinto, "From mode-stirred enclosures to electromagnetic sinai billiards: Chaotic models of reverberation enclosures," in *Proc. 6th Int. Conf. Electromagn. Adv. Appl.*, 1999, pp. 357–360.
[29] F. Haake, *Quantum Signatures of Chaos*. New York: Springer-Verlag, 1991.
[30] M. L. Mehta, *Random Matrices*, 3rd ed. New York: Academic, 2004.
[31] O. Bohigas, M. J. Giannoni, and C. Schmit, "Characterization of chaotic quantum spectra and universality of level fluctuation laws," *Phys. Rev. Lett.*, vol. 52, no. 1, pp. 1–4, Jan. 1984.
[32] Y. V. Fyodorov, D. V. Savin, and H.-J. Sommers, "Scattering, reflection and impedance of waves in chaotic and disordered systems with absorption," *J. Phys. A: Math. General*, vol. 38, no. 49, p. 10731, 2005.
[33] S. Hemmady, "A wave-chaotic approach to predicting and measuring electromagnetic field quantities in complicated enclosures," Ph.D. dissertation, Univ. Maryland, College Park 2006. [Online]. Available: http://drum.lib.umd.edu/handle/1903/3979
[34] L. Warne, K. Lee, H. Hudson, W. Johnson, R. Jorgenson, and S. Stronach, "Statistical properties of linear antenna impedance in an electrically large cavity," *IEEE Trans. Antennas Propag.*, vol. 51, no. 5, pp. 978–992, May 2003.
[35] W. A. Johnson, L. K. Warne, R. E. Jorgenson, and K. S. H. Lee, "An improved statistical model for linear antenna input impedance in an electrically large cavity," Sandia National Lab., Albuquerque, NM, Tech. Rep. SAND2005-1505, 2005.
[36] D. M. Pozar, *Microwave Engineering*, 2nd ed. New York: Wiley, 2004.
[37] T. M. Antonsen, G. Gradoni, E. Ott, and S. M. Anlage, in *Proc. IEEE Int. Symp. Electromagn. Compat.*, 2011, pp. 220–225.
[38] E. C. Jordan and K. G. Balmain, *Electromagnetic Waves and Radiating Systems*. London, U.K.: Technical Publications, 1968.
[39] S. Ramo, J. R. Whinnery, and T. Van Duzer, *Fields and Waves in Communication Electronics*. vol. 2. New York: Wiley, 1994.
[40] C. A. Balanis, *Antenna Theory: Analysis and Design*. New York: Wiley-Interscience, 2005.
[41] P. Bhatria, I. Bahl, R. Garg, and A. Ittipiboon, *Microstrip Antenna Design Handbook*. Norwood, MA: Artech House, 2001.
[42] A. Peterson, S. Ray, and R. Mittra, *Computational Methods for Electromagnetics (IEEE Press Series on Electromagnetic Wave Theory*. Wiley-IEEE Press; 1 edition, Dec. 1997.
[43] E. S. Siah, K. Sertel, J. Volakis, V. Liepa, and R. Wiese, "Coupling studies and shielding techniques for electromagnetic penetration through apertures on complex cavities and vehicular platforms," *IEEE Trans. Electromagn. Compat.*, vol. 45, no. 2, pp. 245–257, May 2003.
[44] C. Xiuqiao, H. Yihua, Z. Jianhua, H. Yourui, and H. Li, "The simulation of electromagnetic pulse coupling with computer box," in *Proc. 3rd Int. Conf. Comput. Electromagn. Appl.*, Nov. 2004, pp. 260–263.
[45] S. Georgakopoulos, C. Birtcher, and C. Balanis, "HIRF penetration through apertures: FDTD versus measurements," *IEEE Trans. Electromagn. Compat.*, vol. 43, no. 3, pp. 282–294, Aug. 2001.
[46] (2008). [Online]. Available: http://www.cst.com/content/applications/article/article.aspx?id=205
[47] T. Wittig, T. Weiland, F. Hirtenfelder, and W. Eurskens. (Jan. 2001). Efficient parameter extraction of high-speed ic-interconnects based on 3d field simulations using fit. in *Proc. Int. Zürich Symp. Tech. Exhib. Electromagn. Comp.,* pp. 281–286 [Online]. Available: http://www.hirtenfelder.curacao-dreams.com/SPICE_Paper_Tilmann_332.pdf
[48] M. Capstick, J. Jekkonen, A. Marvin, I. Flintoft, and L. Dawson, "A novel indirect method to determine the radiation impedance of a handheld antenna structure," *IEEE Trans. Instrum. Meas.*, vol. 58, no. 3, pp. 578–585, Mar. 2009.
[49] J. A. Hart, T. M. Antonsen, and E. Ott, "The effect of short ray trajectories on the scattering statistics of wave chaotic systems," *Phys. Rev. E—Statist., Nonlinear Soft Matter Phys.*, vol. 80, no. 4, pt. 1, p. 041109, 2009.
[50] J. H. Yeh, J. A. Hart, E. Bradshaw, T. M. Antonsen, E. Ott, and S. M. Anlage, "Determination of universal and non-universal properties of wave chaotic scattering systems," *Phys. Rev. E—Statist., Nonlinear Soft Matter Phys.*, vol. 81, p. 025201(R), 2010.
[51] J.-H. Yeh, J. A. Hart, E. Bradshaw, T. M. Antonsen, E. Ott, and S. M. Anlage, "Experimental examination of the effect of short ray trajectories in two-port wave-chaotic scattering systems," *Phys. Rev. E—Statist., Nonlinear Soft Matter Phys.*, vol. 82, p. 041114, 2010.
[52] U. Kuhl, M. Martínez-Mares, R. A. Méndez-Sánchez, and H.-J. Stöckmann, "Direct processes in chaotic microwave cavities in the presence of absorption," *Phys. Rev. Lett.*, vol. 94, no. 14, p. 144101, 2005.
[53] H. Schanze, H.-J. Stöckmann, M. Martínez-Mares, and C. H. Lewenkopf, "Universal transport properties of open microwave cavities with and without time-reversal symmetry," *Phys. Rev. E—Statist., Nonlinear Soft Matter Phys.*, vol. 71, no. 1, pt. 2, p. 016223, 2005.
[54] X. Zheng, S. Hemmady, T. M. Antonsen, S. M. Anlage, and E. Ott, "Characterization of fluctuations of impedance and scattering matrices in wave chaotic scattering," *Phys. Rev. E—Statist., Nonlinear Soft Matter Phys.*, vol. 73, no. 4, pt. 2, p. 6, 2006.
[55] S. Hemmady, X. Zheng, T. M. Antonsen, E. Ott, and S. M. Anlage, "Aspects of the scattering and impedance properties of chaotic microwave cavities," *Acta Physica Polonica*, vol. 109, no. 1, p. 5, 2005.
[56] H. V. Tran, Z. B. Drikas, T. D. Andreadis, Y. J.-H., and S. M. Anlage, "Application of the random coupling model to the calculation of electromagnetic statistics in complex enclosures," to be published.
[57] D.-H. Wu, J. S. A. Bridgewater, A. Gokirmak, and S. M. Anlage (1998), "Probability amplitude fluctuations in experimental wave chaotic eigenmodes with and without time-reversal symmetry," *Phys. Rev. Lett.*, vol. 81, no. 14, p. 2890, 1998.
[58] E. J. Heller, "Bound-state eigenfunctions of classically chaotic hamiltonian systems: Scars of periodic orbits," *Phys. Rev. Lett.*, vol. 53, no. 16, pp. 1515–1518, Oct. 1984.
[59] T. M. Antonsen, E. Ott, Q. Chen, and R. N. Oerter, "Statistics of wavefunction scars," *Phys. Rev. E*, vol. 51, no. 1, pp. 111–121, Jan. 1995.
[60] L. K. Warne, R. E. Jorgenson, J. D. Kotulski, and K. S. H. Lee, "Two dimensional unstable scar statistics," Sandia National Lab., Albuquerque, NW, Sandia Rep. SAND2006-7511, 2006.
[61] C. Fiachetti and B. Michielsen, "Electromagnetic random field models for analysis of coupling inside mode tuned chambers," *Electron. Lett.*, vol. 39, no. 24, pp. 1713–1714, Nov. 2003.
[62] G. Gradoni, J.-H. Yeh, T. M. Antonsen, S. M. Anlage, and E. Ott, "Wave chaotic analysis of weakly coupled reverberation chambers," in *Proc. IEEE Electromagn. Compat. Symp.*, 2011, pp. 202–207.
[63] L. M. Pecora, H. Lee, D.-H. Wu, T. Antonsen, M.-J. Lee, and E. Ott, "Chaos regularization of quantum tunneling rates," *Phys. Rev. E*, vol. 83, no. 6, p. 065201, Jun. 2011.

Sameer Hemmady (M'08) received the B.S. degree in electronics engineering from the University of Mumbai, Mumbai, India, in 2002, and the M.S. degree in telecommunications engineering and the Ph.D. degree in electrical engineering both from the University of Maryland, College Park, in 2004 and 2006, respectively.

He is an Applied Physicist with more than 10 years' experience in the planning, design, implementation, and technical assessment of advanced directed energy weaponized systems. He is currently with the TechFlow Scientific, A Division of TechFlow Inc., Albuquerque, NM. He has served as a Program Manager and Principal Investigator on several U.S. Department of Defense programs pertaining to nonlethal directed energy weapons, counter-electronics, and radar technologies. His technical expertise includes intentional electromagnetic interference and compatibility, low-observable phased array antennas, radar systems, Terahertz and optical beam transport systems, and lasers. He is also a Research Professor in the Applied Electromagnetics Group, Department of Electrical and Computer Engineering, University of New Mexico, Albuquerque. He has authored one book on statistical electromagnetism, several journal papers, and conference proceedings covering applied research in wave propagation, statistical electromagnetism, EMI/EMC, and reconfigurable antennas.

Dr. Hemmady received the "IEEE Outstanding Young Engineer Award" from the IEEE Albuquerque Chapter, in 2011.

Thomas M. Antonsen, Jr. (F'12) was born in Hackensack, NJ, in 1950. He received the B.S. degree in electrical engineering in 1973, and the M.S. and Ph.D. degrees in electrical engineering in 1976 and 1977, respectively, all from Cornell University, Ithaca, NY.

From 1976 to 1977, he was a National Research Council Postdoctoral Fellow at the Naval Research Laboratory, and from 1977 to 1980, a Research Scientist in the Research Laboratory of Electronics, Massachusetts Institute of Technology. Since 1980, he has been with the University of Maryland, College Park, where in 1984, he was with the Faculty Member in the Departments of Electrical Engineering and Physics, and is currently a Professor in the Departments of Physics and Electrical and Computer Engineering. He has held visiting appointments at the Institute for Theoretical Physics, University of California, Santa Barbara, the Ecole Polytechnique Federale de Lausanne, Lausanne, Switzerland, and the Institute de Physique Theorique, Ecole Polytechnique, Palaiseau, France. From 1998 to 2000, he served as the Acting Director in the Institute for Plasma Research, University of Maryland. He is the author and coauthor of more than 350 journal articles and the coauthor of the book "*Principles of Free-Electron Lasers*." His research interests include the theory of magnetically confined plasmas, the theory and design of high power sources of coherent radiation, nonlinear dynamics in fluids, and the theory of the interaction of intense laser pulses and plasmas.

Dr. Antonsen was selected as a Fellow of the Division of Plasma Physics of the American Physical Society, in 1986. In 1999, he was a corecipient of the Robert L. Woods Award for Excellence in the Vacuum Electronics Technology, and in 2003, he received the IEEE Plasma Science and Applications Award. In 2004, he was given the Outstanding Faculty Research Award of the Clark School of Engineering. In 2010, he served as the Chair of the Division of Plasma Physics of the American Physical Society. He has served on the editorial board of Physical Review Letters, The Physics of Fluids, and Comments on Plasma Physics.

Edward Ott (LF'11) received the B.S. degree in electrical engineering from The Cooper Union, New York, NY, in 1963, and the M.S. and Ph.D. degrees in electrophysics both from Polytechnic Institute of Brooklyn, Brooklyn, NY, in 1965 and 1967, respectively.

After receiving the Ph.D. degree, he became an NSF Postdoctoral Fellow in the Department of Applied Mathematics and Theoretical Physics, Cambridge University. Following his Postdoctoral research work, he was appointed as an Assistant Professor in the Department of Electrical Engineering at Cornell University, where he eventually became a Full Professor. In 1979, he moved from Cornell University to take up his current position as a Professor of physics and electrical engineering, University of Maryland, College Park, where he currently holds the title of a Distinguished University Professor. His current research interest includes the area of chaos and nonlinear dynamics.

Steven M. Anlage (M'94) received the B.S. degree in physics from the Rensselaer Polytechnic Institute, Troy, NY, in 1982, and the M.S. and Ph.D. degrees in applied physics from the California Institute of Technology, Pasadena, in 1984 and 1988, respectively. His graduate research concerned the physics and materials properties of quasicrystals. He was a Postdoctoral Researcher with the Beasley-Geballe-Kapitulnik Group, Stanford University, from 1987 to 1990, where his research was focused on high-frequency properties of high temperature superconductors, including both basic physics and applications to tunable microwave devices.

He is a Professor of physics and a Faculty Affiliate in the Department of Electrical and Computer Engineering, University of Maryland, College Park. In 1990, he was appointed as an Assistant Professor of physics in the Center for Superconductivity Research, University of Maryland, where in 1997, he became an Associate Professor, and a Full Professor of physics in 2002. He was the Interim Director of the Center for Nanophysics and Advanced Materials from 2007 to 2009. In 2008, he was appointed as a Research Professor of the National Security Institute at the Naval Postgraduate School, Monterey, CA. In 2011, he was appointed as a Research Professor at the DFG-Center for Functional Nanostructures, Karlsruhe Institute of Technology, Karlsruhe, Germany. He is a member of the Maryland NanoCenter, where his research in high-frequency superconductivity has addressed questions of the pairing state symmetry of the cuprate superconductors, the dynamics of conductivity fluctuations and vortices, and microwave applications such as superconducting negative index of refraction metamaterials. He has also developed and patented a near-field scanning microwave microscope for quantitative local measurements of electronic materials (dielectrics, semiconductors, metals, and superconductors) down to nanometer length scales. He also performs microwave analog experiments of the Schrödinger equation to test fundamental theories of quantum chaos. As part of this research, he has developed a statistical prediction model for effects of high-power microwave signals on electronics. He is also active in the emerging field of time-reversed electromagnetics. He has co-authored more than 140 research papers in scientific journals.

Dr. Anlage is a member of the American Physical Society, the Optical Society of America, and the Materials Research Society. His research is funded by the National Science Foundation and DoD, and he is an Active Consultant to the U.S. Government. He was a member of the NSF-funded Materials Research Science and Engineering Center at the University of Maryland from 1995 to 2005.